Editors' Suggestion

Direct Visualization of Surface Spin-Flip Transition in $MnBi_4Te_7$

Wenbo Ge,[1] Jinwoong Kim,[1] Ying-Ting Chan,[1] David Vanderbilt,[1] Jiaqiang Yan,[2] and Weida Wu[1,*]
[1]Department of Physics and Astronomy, Rutgers University, Piscataway, New Jersey 08854, USA
[2]Materials Science and Technology Division, Oak Ridge National Laboratory, Oak Ridge, Tennessee 37831, USA

(Received 16 April 2022; revised 23 June 2022; accepted 9 August 2022; published 1 September 2022)

We report direct visualization of spin-flip transition of the surface layer in antiferromagnet $MnBi_4Te_7$, a natural superlattice of alternating $MnBi_2Te_4$ and Bi_2Te_3 layers, using cryogenic magnetic force microscopy (MFM). The observation of magnetic contrast across domain walls and step edges confirms that the antiferromagnetic order persists to the surface layers. The magnetic field dependence of the MFM images reveals that the surface magnetic layer undergoes a first-order spin-flip transition at a magnetic field that is lower than the bulk transition, in excellent agreement with a revised Mills model. Our analysis suggests no reduction of the order parameter in the surface magnetic layer, implying robust ferromagnetism in the single-layer limit. The direct visualization of surface spin-flip transition not only opens up exploration of surface metamagnetic transitions in layered antiferromagnets, but also provides experimental support for realizing quantized transport in ultrathin films of $MnBi_4Te_7$ and other natural superlattice topological magnets.

DOI: 10.1103/PhysRevLett.129.107204

Broken time reversal symmetry and topological band structure are the key ingredients for many interesting phenomena, such as the quantum anomalous Hall (QAH) effect and the topological magnetoelectric effect [1,2]. Although the QAH effect has been demonstrated in ferromagnetic topological insulator (TI) thin films, the inherent disorder from doping results in inhomogeneity that limits the quantization to subkelvin temperatures [3–5]. Intrinsic magnetic TIs provide an alternative approach to combine magnetism and topological band structure in stoichiometric compounds. For example, the Z_2 topological index in *A*-type antiferromagnets is protected by the symmetry of alternating ferromagnetic layers [6].

$MnBi_2Te_4$ is the first tangible candidate for an antiferromagnetic-TI (AFM-TI) [7–9]. The observation of quantum transport in exfoliated flakes provides strong evidence of QAH and axion insulator states in zero magnetic field [10,11], though it remains controversial [12]. Indeed, high-resolution angle-resolved photoemission spectroscopy (ARPES) reports gapless Dirac surface states, suggesting that the surface spin configuration is different from the out-of-plane *A*-type AFM order in bulk [13–16]. Previous magnetic force microscopy (MFM) studies by some of us, however, confirmed that the *A*-type antiferromagnetic order persists to the surface layer of $MnBi_2Te_4$, in agreement with recent ARPES measurements [17,18]. The robust *A*-type antiferromagnetic order is further corroborated by the observation of the long-sought surface spin-flop transition [17].

In spite of mounting evidence of the robust *A*-type AFM order, it is possible that surface relaxation is limited to the very top layer and strictly follows morphology of surface steps so that it escapes the MFM observation. This scenario, however, requires an abrupt transition from ordered to relaxed magnetic states within the septuple layer beneath each step edge. This is physically unlikely given the strong intralayer exchange coupling [19]. If it is true, a further reduction of interlayer coupling by increasing the interlayer separation would favor a stronger surface relaxation effect, which can be visualized by magnetic imaging. The natural superlattice compounds $MnBi_2Te_4-(Bi_2Te_3)_n$ provide the perfect system to test such a hypothesis. In these systems, n layers of Bi_2Te_3 are inserted between $MnBi_2Te_4$ layers, dramatically reducing the interlayer coupling without much impact on the uniaxial anisotropy [20–22]. Thus, the metamagnetic transition becomes a spin-flip transition in $MnBi_4Te_7$ and $MnBi_6Te_{10}$ single crystals [20–23]. ARPES measurements observed gapless Dirac surface states on the $MnBi_2Te_4$ termination, again suggesting strong surface relaxation of the *A*-type AFM order [20,24]. Therefore, it is imperative to probe the surface magnetism of the $MnBi_2Te_4$ termination in $MnBi_4Te_7$. It is also interesting to find out whether there is a surface spin-flip transition preceding the bulk one, which has been predicted theoretically but has evaded experimental observations [25].

In this Letter, we report that the *A*-type AFM order persists to the surface $MnBi_2Te_4$ termination, as illustrated by the termination dependence of the magnetic signal observed by MFM, excluding the previous proposed surface relaxation of the *A*-type AFM order [20,24]. In addition, we discover a first-order spin-flip transition on the $MnBi_2Te_4$ exposed surface that precedes the bulk spin-flip transition, in excellent agreement with a revised Mills model [17,26,27]. Our analysis further reveals no reduction

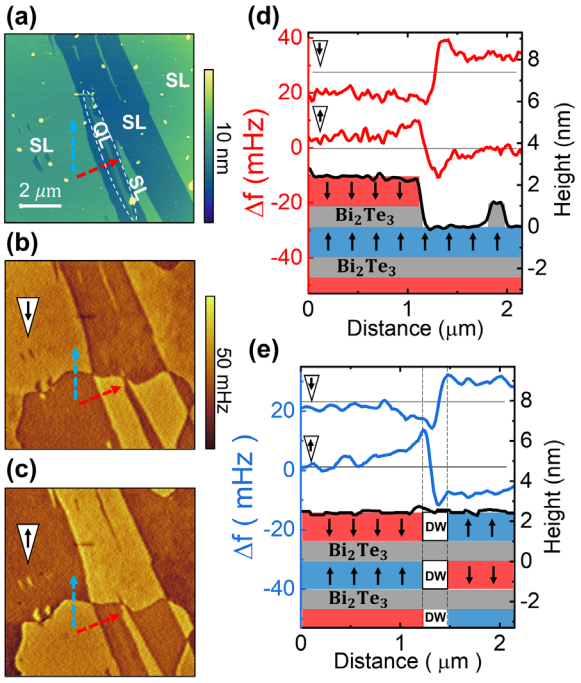

FIG. 1. (a) Topographical image (5.5 K) measured on a cleaved surface of a $MnBi_4Te_7$ single crystal. (b),(c) MFM images (5.5 K, 0 T) measured at the same location with negatively and positively polarized tips, respectively. The domain contrast is reversed as the tip moment is flipped, confirming that the magnetic contrast comes from the sample stray field. A curvilinear domain wall crossing the SL and QL steps is visible in the MFM images. (d),(e) Line profiles of the topographical image (black) and MFM images (red and blue) along the red and blue arrow in (b) and (c). Schematics of crystal and magnetic stacking are sketched under the topographical line profiles. Red and blue layers represent the ferromagnetic SLs with moments pointing down and up, respectively. The gray layers are QLs. The frequency shift line profile is plotted across a SL plus QL step in (d), while it is plotted across the domain wall (DW) on a flat SL layer in (e).

of the magnetization of surface $MnBi_2Te_4$ layer despite the reduced number of neighbors, indicating that the Ising-like ferromagnetism could persist in single-layer $MnBi_2Te_4$ [28]. Therefore, $MnBi_4Te_7$ is a promising material platform for achieving high-temperature quantized transport in few-layer thin films [29].

$MnBi_4Te_7$ single crystals are grown out of Bi_2Te_3 flux (see Supplemental Material [30]). Samples are cleaved in ambient condition to expose fresh surfaces before being mounted to a cryogenic MFM [17,31]. The thickness of samples ranges from 25 to 150 μm. Because of the natural superlattice structure, the surface terminates at either $MnBi_2Te_4$ septuple layer (SL) or Bi_2Te_3 quintuple layer (QL). Figure 1 shows the typical topography of a cleaved surface of a $MnBi_4Te_7$ single crystal [30]. A trench with step height ~2.4 nm cuts through the field of view. The step height is approximately the c-axis lattice constant, indicating that it consists of a $MnBi_2Te_4$ SL and a Bi_2Te_3 QL. There are also a few islands inside the trench. Along the red arrow in Fig. 1(a), there is an island with height of ~1.1 nm highlighted by a dashed ellipse, indicating it is a QL. Therefore, the majority of the surface is the $MnBi_2Te_4$ termination. Figure 1(d) shows the corresponding topographical line profile with a cartoon of the stacking order.

Figures 1(b) and 1(c) show the MFM image measured with opposite tip moments at 5.5 K in zero external magnetic field. The tip moment is reversed by applying a 0.1 T external field, which is small enough without affecting the domain pattern, but large enough to reverse the MFM tip moment. The bulk spin-flip transition is ~0.13 T, while the coercive field of MFM tip moment is ~0.04 T [30]. The reversal of the MFM contrast with tip moment orientation confirms the magnetic signal is from the stray field of the sample. A curvilinear domain wall separating antiphase domains cuts across the trench. The MFM contrast reverses across the domain wall (blue arrow) or across the step on the same side of the domain wall (red arrow). The alternating MFM signal across both the domain wall and the step confirms that the out-of-plane A-type AFM order persists all the way to the surface $MnBi_2Te_4$ layer. The topographic and MFM line profiles with the corresponding magnetic structures are shown in Figs. 1(d) and 1(e) (see Supplemental Material [30]). The absence of magnetic contrast on Bi_2Te_3 island suggests its magnetic signal is negligible at 5.5 K and higher temperatures even though Mn_{Bi} defects in Bi_2Te_3 carry magnetic moments [32]. Thus, the Bi_2Te_3 layer behaves as a nonmagnetic spacer in $MnBi_4Te_7$. Thus, the magnetic contrast observed in this work originates from the magnetic order in the $MnBi_2Te_4$ layers. At lower temperatures, the magnetism in Bi_2Te_3 layers could interact with the AFM order in $MnBi_2Te_4$ layers, which might be related to the substantial hysteresis loop of the bulk spin-flip transition [20–22,33]. The persistence of out-of-plane A-type AFM order suggests that $MnBi_4Te_7$ is a perfect system to explore the surface metamagnetic transition, similar to the surface spin-flop transition observed in $MnBi_2Te_4$ single crystals [17].

In $MnBi_4Te_7$, the insertion of the Bi_2Te_3 layer dramatically reduces the interlayer exchange interaction without affecting the uniaxial magnetic anisotropy. Therefore, the metamagnetic transition becomes a spin-flip transition [20–22]. The bulk spin-flip (BSF) transition field is $\mu_0 H_{BSF} \approx 0.13$ T at 5.5 K, in good agreement with recent MFM studies [30,35]. Thus, the surface $MnBi_2Te_4$ layer with antiparallel moment is expected to undergo a surface spin-flip transition before the bulk transition because of a reduction of the Weiss field due to the missing of half of the nearest neighbors [25]. Figures 2(a)–2(f) show selected MFM images measured at various out-of-plane magnetic fields after 0.01 T field cooling through the Néel temperature ($T_N \approx 13$ K) [22]. Positive field value indicates the direction of the field is up. Curvilinear domain walls separating $\alpha(\uparrow\downarrow\uparrow\downarrow)$ and $\beta(\downarrow\uparrow\downarrow\uparrow)$ antiphase domains

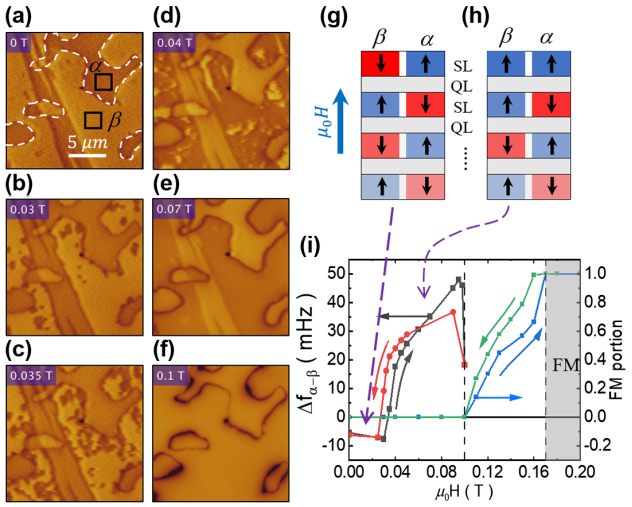

FIG. 2. (a)–(f) Selected MFM images taken at 5.5 K with increasing magnetic fields, which are labeled on the corner of each image. The color scales from (a) to (f) are 0.06, 0.11, 0.12, 0.12, 0.26 and 3 Hz, respectively. The AFM domain walls are traced out with dashed lines in (a). The boxed areas α and β in (a) corresponds to parallel and antiparallel surfaces, respectively. (g),(h) Magnetic structures of areas α and β before and after the surface spin-flip transition, respectively. (i) H dependence of MFM contrast between areas α and β and that of forced ferromagnetic (FM) domain population during the BSF transition (between 0.1 and 0.17 T). The colored arrows indicate the field sweeping direction. Above 0.17 T, the system is in the FM state.

are highlighted in Fig. 2(a). The spin configurations of two types of antiphase domains are illustrated in Fig. 2(g). As the magnetic field is increased to 0.03 T, a few bubblelike features with dark contrast appear only on antiparallel surfaces (β domains above the trench) as shown in Fig. 2(b), indicating a metamagnetic transition that precedes the bulk spin-flip transition. More dark features nucleate and expand with further increasing magnetic field. The dark contrast takes over the whole antiparallel surface at 0.07 T as shown in Figs. 2(b)–2(e). After that, the magnetic contrast between two surface terminations (parallel and antiparallel) is reversed, as summarized in Fig. 2(i) [30]. Since the transition only happens on the antiparallel surface, it is the long-sought surface spin-flip (SSF) transition [25]. The first-order nature of the SSF transition is further corroborated by the small hysteresis between increasing and reducing field results shown in Fig. 2(i). Note that the magnetic contrast of AFM domains is much (~1000 times) weaker than that between the AFM and the forced ferromagnetic phases in the BSF transition, further corroborating that the observed domain process is the transition of the surface layers [30]. The BSF transition is characterized by the increase of areal fraction of the forced ferromagnetic phase [34]. The magnetic structure of the boxed region before and after the SSF transition is shown in Figs. 2(g) and 2(h). Consistently, the same SSF transition is observed on the opposite termination (α domains above the trench) with negative (downward) magnetic fields [30], confirming the SSF transition is an intrinsic phenomenon of the surface layer with moment antiparallel to the external field. Similar to prior MFM studies of $MnBi_2Te_4$, the magnetic contrast of domain walls linearly increases with increasing magnetic field at small fields, suggesting a susceptibility contrast mechanism [17,35].

The observed surface spin-flip transition field ($\mu_0 H_{\mathrm{SSF}}$) is approximately 1/4 of that of the bulk one. We observed a similar ratio in different samples with slightly different transition temperature and fields (see Supplemental Material [30]). Furthermore, the ratio does not vary much for $T < 10$ K (~80% of T_N), suggesting that the SSF transition follows the BSF one. To understand the mechanism of SSF transition, we performed an analysis using a revised Mills model in the high anisotropy limit ($K/J \gg 1$). Here K is the uniaxial anisotropy energy and J is the exchange energy [6,36,37]. In comparison, the previous modeling of the surface spin-flop transition in $MnBi_2Te_4$ is in the low anisotropy limit ($K/J \ll 1$) [17]. Therefore, in contrast to the claim of recent MFM studies [35], there is no surface spin-flop transition in $MnBi_4Te_7$.

The Mills model is effectively a one-dimensional spin chain model where each spin represents the magnetic moment of each layer in A-type AFMs [26]. The strong uniaxial anisotropy ($K/J \gg 1$) forces all spins to align on the vertical easy axis. In this limit, the anisotropy term can be omitted from the original model, and the total energy is simplified to $E = J\sum_{i=1}^{N-1} \boldsymbol{S}_i \cdot \boldsymbol{S}_{i+1} - \sum_{i=1}^{N} \boldsymbol{S}_i \cdot \boldsymbol{h}$. Thus, the total energy of the AFM ground state is $E_{\mathrm{AFM}} = -(N - 3 + 2\lambda_J\lambda_S)J$, where λ_J is the ratio of the revised surface exchange coupling to the bulk one, and λ_S is the ratio of the revised surface spin moment to that in bulk [6]. Here, λ_J and λ_S are phenomenological parameters that characterize the effect of surface relaxation. The E_{AFM} is independent of external field because of compensated magnetic moments. If the surface layer or the second layer moment reverses, the Zeeman energy gain of the uncompensated moments would result in first-order transitions. Figure 3(a) shows the total energies of four spin states for $\lambda_J\lambda_S < 1$. The schematics are shown in Fig. 3(c). First-order phase transitions occur at threshold fields of $h_1 = \lambda_J J$, $h_2 = (1 + \lambda_J\lambda_S)J$, and $h_3 = 2J$, where the lowest total energy evolves from the AFM state to the force ferromagnetic state via the SSF and second-layer spin-flip (SLSF) states. Note that the h_1 only depends on λ_J. As discussed earlier, the ratio $H_{\mathrm{SSF}}/H_{\mathrm{BSF}}$ is approximately 1/4, which is h_1/h_3 in our model. Thus, the ratio of revised surface exchange can be estimated as $\lambda_J = 2h_1/h_3 \approx 0.5$. In other words, the exchange coupling between the surface layer and the next layer is approximately half of the value in bulk of $MnBi_4Te_7$, probably due to surface relaxation effect. Interestingly, the revised Mills model also predicts a second-layer spin-flip transition (h_2) between the SSF

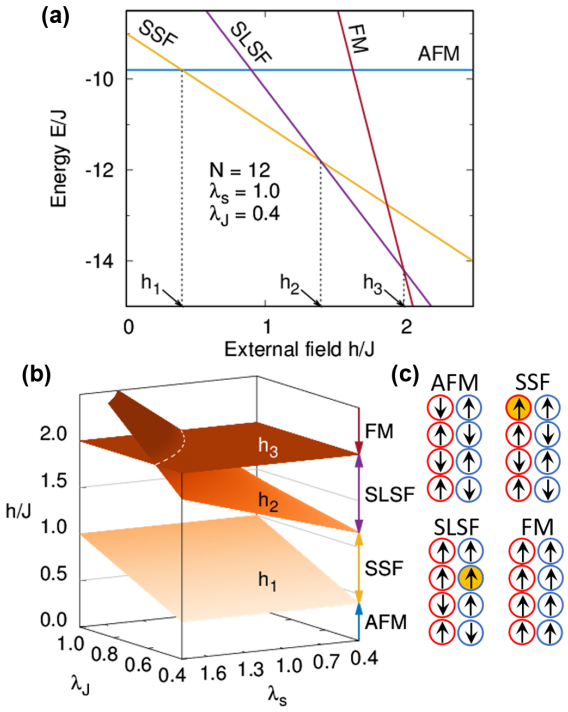

FIG. 3. (a) Total energy as a function of exchange field, for the four magnetic phases with 12 spin-lattice sites ($N = 12$) and reduced surface exchange coupling ($\lambda_J = 0.4$). First-order phase transitions are expected at the crossing points h_1, h_2, and h_3, which are SSF, SLSF, and bulk spin-flip transitions, respectively. (b) The crossing points with respect to the surface exchange coupling λ_J and the surface spin moment λ_S. The SLSF phase can appear only when the surface parameters are reduced as $\lambda_J\lambda_S < 1$. (c) Schematic illustration of the surface spin-flip states where red and blue represent antiphase domains. Assuming the external field points up, SSF (SLSF) occurs at the first (second) layer of the antiparallel (parallel) surface as highlighted by orange filling.

transition (h_1) and the bulk transition (h_3) for $\lambda_J\lambda_S < 1$, Otherwise the total energy of the SLSF phase is always above the lowest energy states [30] so that the system undergoes a phase transition from SSF to FM states above a threshold field of $h_{\mathrm{SSF-FM}} = 2[(N-3+\lambda_J\lambda_S)/(N-2)]J$, which approaches h_3 in the bulk limit ($N \to \infty$). Experimentally, no signature of the SLSF transition is observed before the bulk spin-flip transition begins (~0.1 T), indicating $\lambda_J\lambda_S \geq 1$. However, the SLSF transition might be hidden by the relatively broad (~0.07 T) BSF transition.

To explore whether the SLSF transition is overshadowed by the BSF transition, we performed field "annealing" experiments by carefully increasing the magnetic field to induce partial but reversible BSF transition ($\mu_0 H \leq 0.14$ T) [30]. For the negative field, the surface of α domains undergo SSF transition at −0.033 T (see Supplemental Material [30]). Figure 4(a) shows the MFM image taken at −0.09 T after sweeping the magnetic field to −0.1 T. Interestingly, numerous small patches with dark contrast

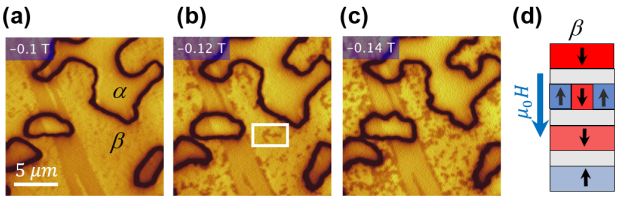

FIG. 4. (a)–(c) MFM images taken at −0.09 T after external magnetic field was increased to the set values labeled at the upper-left corners. The color scale is 0.2 Hz. The field annealing results illustrate partial SLSF transition on the parallel surface. (d) Schematic illustration of SLSF phase. The magnetic moment in the second SL of the β domain is partially flipped, which corresponds to the dark patches as highlighted in the white box in (b).

appear on the parallel surface, indicating a partial SLSF transition. As shown in Figs. 4(b) and 4(c), more fractions of β domains undergo partial SLSF transition with increasing fraction of dark patches after −0.12 and −0.14 T field annealing. So the SLSF transition field is very close to that of the BSF transition, i.e., $h_2 \approx h_3$, indicating $\lambda_S \approx 2$. Because of the large uncertainty in estimating h_2, the estimated value λ_S suggests that surface magnetization is comparable with the bulk value. Thus, surface relaxation does not degrade the order parameter of the surface $MnBi_2Te_4$ layer, indicating that a robust 2D ferromagnetism could persist in the single-layer $MnBi_2Te_4$ limit, which is favorable for exploring the quantum transport in thin films or flakes of $MnBi_4Te_7$ and related superlattice compounds [29].

In summary, we discover the SSF transition in AFM-TI $MnBi_4Te_7$, in good agreement with a revised Mills model. Furthermore, we observed a partial SLSF transition, suggesting robust magnetization in the surface $MnBi_2Te_4$ layer. The alternating domain contrast across the domain wall or step edge observed in $MnBi_4Te_7$ unambiguously confirms the persistence of A-type AFM order to the surface $MnBi_2Te_4$ layer. The discovery and direct visualizing of SSF transition paves the way for exploring surface or two-dimensional magnetic states of functional AFMs for spintronic applications [38]. Moreover, the robust ferromagnetism in the single-layer limit opens the door to realizing QAH or axion insulator states in the ultrathin films of the natural superlattice $MnBi_4Te_7$ and related compounds [20,21,29].

The MFM studies at Rutgers are supported by the Office of Basic Energy Sciences, Division of Materials Sciences and Engineering, U.S. Department of Energy under Award No. DE-SC0018153. The simulation efforts are supported by NSF Grant No. DMR-1954856. Work at ORNL was supported by the U.S. Department of Energy, Office of Science, Basic Energy Sciences, Materials Sciences and Engineering Division.

*wdwu@physics.rutgers.edu

[1] C.-Z. Chang *et al.*, Science **340**, 167 (2013).
[2] D. Xiao, J. Jiang, J.-H. Shin, W. Wang, F. Wang, Y.-F. Zhao, C. Liu, W. Wu, M. H. W. Chan, N. Samarth, and C.-Z. Chang, Phys. Rev. Lett. **120**, 056801 (2018).
[3] E. O. Lachman, A. F. Young, A. Richardella, J. Cuppens, H. R. Naren, Y. Anahory, A. Y. Meltzer, A. Kandala, S. Kempinger, Y. Myasoedov, M. E. Huber, N. Samarth, and E. Zeldov, Sci. Adv. **1**, e1500740 (2015).
[4] C.-Z. Chang, W. Zhao, D. Y. Kim, H. Zhang, B. A. Assaf, D. Heiman, S.-C. Zhang, C. Liu, M. H. W. Chan, and J. S. Moodera, Nat. Mater. **14**, 473 (2015).
[5] A. J. Bestwick, E. J. Fox, X. Kou, L. Pan, K. L. Wang, and D. Goldhaber-Gordon, Phys. Rev. Lett. **114**, 187201 (2015).
[6] R. S. K. Mong, A. M. Essin, and J. E. Moore, Phys. Rev. B **81**, 245209 (2010).
[7] M. M. Otrokov, I. P. Rusinov, M. Blanco-Rey, M. Hoffmann, A. Y. Vyazovskaya, S. V. Eremeev, A. Ernst, P. M. Echenique, A. Arnau, and E. V. Chulkov, Phys. Rev. Lett. **122**, 107202 (2019).
[8] M. M. Otrokov *et al.*, Nature (London) **576**, 416 (2019).
[9] J. Li, Y. Li, S. Du, Z. Wang, B.-L. Gu, S.-C. Zhang, K. He, W. Duan, and Y. Xu, Sci. Adv. **5**, eaaw5685 (2019).
[10] Y. Deng, Y. Yu, M. Z. Shi, Z. Guo, Z. Xu, J. Wang, X. H. Chen, and Y. Zhang, Science **367**, 895 (2020).
[11] C. Liu, Y. Wang, H. Li, Y. Wu, Y. Li, J. Li, K. He, Y. Xu, J. Zhang, and Y. Wang, Nat. Mater. **19**, 522 (2020).
[12] D. Ovchinnikov, X. Huang, Z. Lin, Z. Fei, J. Cai, T. Song, M. He, Q. Jiang, C. Wang, H. Li, Y. Wang, Y. Wu, D. Xiao, J.-H. Chu, J. Yan, C.-Z. Chang, Y.-T. Cui, and X. Xu, Nano Lett. **21**, 2544 (2021).
[13] Y. J. Chen *et al.*, Phys. Rev. X **9**, 041040 (2019).
[14] Y.-J. Hao *et al.*, Phys. Rev. X **9**, 041038 (2019).
[15] H. Li *et al.*, Phys. Rev. X **9**, 041039 (2019).
[16] P. Swatek, Y. Wu, L.-L. Wang, K. Lee, B. Schrunk, J. Yan, and A. Kaminski, Phys. Rev. B **101**, 161109(R) (2020).
[17] P. M. Sass, J. Kim, D. Vanderbilt, J. Yan, and W. Wu, Phys. Rev. Lett. **125**, 037201 (2020).
[18] D. Nevola, H. X. Li, J.-Q. Yan, R. G. Moore, H.-N. Lee, H. Miao, and P. D. Johnson, Phys. Rev. Lett. **125**, 117205 (2020).
[19] B. Li, J.-Q. Yan, D. M. Pajerowski, E. Gordon, A.-M. Nedić, Y. Sizyuk, L. Ke, P. P. Orth, D. Vaknin, and R. J. McQueeney, Phys. Rev. Lett. **124**, 167204 (2020).
[20] C. Hu, K. N. Gordon, P. Liu, J. Liu, X. Zhou, P. Hao, D. Narayan, E. Emmanouilidou, H. Sun, Y. Liu, H. Brawer, A. P. Ramirez, L. Ding, H. Cao, Q. Liu, D. Dessau, and N. Ni, Nat. Commun. **11**, 97 (2020).
[21] J. Wu, F. Liu, M. Sasase, K. Ienaga, Y. Obata, R. Yukawa, K. Horiba, H. Kumigashira, S. Okuma, T. Inoshita, and H. Hosono, Sci. Adv. **5**, eaax9989 (2019).
[22] J.-Q. Yan, Y. H. Liu, D. S. Parker, Y. Wu, A. A. Aczel, M. Matsuda, M. A. McGuire, and B. C. Sales, Phys. Rev. Mater. **4**, 054202 (2020).
[23] I. I. Klimovskikh *et al.*, npj Quantum Mater. **5**, 54 (2020).
[24] X. Wu *et al.*, Phys. Rev. X **10**, 031013 (2020).
[25] U. K. Rößler and A. N. Bogdanov, Phys. Status Solidi C **1**, 3297 (2004).
[26] D. L. Mills, Phys. Rev. Lett. **20**, 18 (1968).
[27] R. W. Wang, D. L. Mills, E. E. Fullerton, J. E. Mattson, and S. D. Bader, Phys. Rev. Lett. **72**, 920 (1994).
[28] S. Yang, X. Xu, Y. Zhu, R. Niu, C. Xu, Y. Peng, X. Cheng, X. Jia, Y. Huang, X. Xu, J. Lu, and Y. Ye, Phys. Rev. X **11**, 011003 (2021).
[29] H. Sun, B. Xia, Z. Chen, Y. Zhang, P. Liu, Q. Yao, H. Tang, Y. Zhao, H. Xu, and Q. Liu, Phys. Rev. Lett. **123**, 096401 (2019).
[30] See Supplemental Material at http://link.aps.org/supplemental/10.1103/PhysRevLett.129.107204 for topography, complete MFM dataset, and additional information.
[31] P. M. Sass, W. Ge, J. Yan, D. Obeysekera, J. J. Yang, and W. Wu, Nano Lett. **20**, 2609 (2020).
[32] Y. S. Hor, P. Roushan, H. Beidenkopf, J. Seo, D. Qu, J. G. Checkelsky, L. A. Wray, D. Hsieh, Y. Xia, S.-Y. Xu, D. Qian, M. Z. Hasan, N. P. Ong, A. Yazdani, and R. J. Cava, Phys. Rev. B **81**, 195203 (2010).
[33] C. Hu, M. A. Tanatar, R. Prozorov, and N. Ni, J. Phys. D **55**, 054003 (2021).
[34] W. Ge, P. M. Sass, J. Yan, S. H. Lee, Z. Mao, and W. Wu, Phys. Rev. B **103**, 134403 (2021).
[35] J. Guo, H. Wang, X. Wang, S. Gu, S. Mi, ShiyuZhu, J. Hu, F. Pang, W. Ji, H. Gao, T. Xia, and Z. Cheng, arXiv:2112.02320.
[36] L. Fu, C. L. Kane, and E. J. Mele, Phys. Rev. Lett. **98**, 106803 (2007).
[37] R. W. Wang and D. L. Mills, Phys. Rev. B **50**, 3931 (1994).
[38] V. Baltz, A. Manchon, M. Tsoi, T. Moriyama, T. Ono, and Y. Tserkovnyak, Rev. Mod. Phys. **90**, 015005 (2018).